Contents lists available at ScienceDirect

Journal of Wind Engineering & Industrial Aerodynamics

journal homepage: http://ees.elsevier.com

Wind loads on solar panels mounted on flat roofs: Effect of geometric scale

Hatem Alrawashdeh*, Ted Stathopoulos

Department of Building, Civil and Environmental Engineering, Concordia University, Montreal, Quebec, Canada

ARTICLE INFO

Keywords
Codes and standards
Design
Scaling
Solar panels
Wind pressures
Wind tunnel

ABSTRACT

The paper outlines a set of experimental criteria implemented to examine the influence of geometric scale on wind-induced pressures on roof-mounted solar panels tested in a simulated atmospheric boundary layer. The results of this research contribute significantly to the understanding of the obstacles hindering the reliable evaluation of wind loads on solar panels, bearing in mind that the size of wind tunnel models of such structures is a key stumbling block to conducting experiments and getting reliable results. The effect of such shortcomings in the codification process is examined. Three models of geometric ratios 1:50, 1:100 and 1:200 were designed, manufactured and tested in the atmospheric boundary layer wind tunnel of Concordia University. The results show that the geometric test scaling is an important parameter in simulating solar panel models in atmospheric boundary layer wind tunnels, particularly when considering design wind loads.

1. Introduction

Solar power, arguably the most accessible and prevalent application for renewable energy, becomes the focus of world attention resulting in rapid applications of photovoltaic solar panels of various utility-scale systems throughout the world. Furthermore, moving towards renewable energy would offer economic benefits at the individual owner and the national level. Today, solar panels are increasingly used in low-rise residential and industrial buildings with a variety of installations and geometries, mainly recognized in two groups according to their mounting system as: Building Attached Photovoltaics (BAPVs) and Building-Integrated Photovoltaics (BIPVs). In BIPVs installations, PV modules are integrated into the building envelope or components (i.e., roof, façade or windows) instead of using conventional building materials. Therefore, BIPVs are considered as part of the structural envelope system of buildings. On the other hand, PV modules are fixed onto the building walls or roofs in BAPVs installations (i.e., tilted-up on flat roofs, flushed in parallel to inclined roofs or mounted on walls) – as illustrated in Fig. 1, which summarizes various possible installations of BAPVs. In this kind of application, PV systems are not considered as parts of the structural system of the building but they are deemed to be attachments to the building envelope.

The arrays of roof-mounted solar panels from a structural perspective should be designed to withstand at least the array self-weight in addition to other dead loads (electrical system and other attachments), weight of snow built-up and wind pressures induced on the surface. Solar panel systems are lightweight structures and wind pressures on their surfaces, unless considered properly, may lead to damaging or deforming the array. Therefore, the design requirement for solar panels on buildings against wind pressures should satisfy the safety of the PV module cover plate from cracking due to local wind loads, the solar modules from losing or peeling out from their supports due to wind loads applied to the area of the module and the array supporting system from damaging or collapsing due to the wind pressures acting on the panel or array area.

It has been demonstrated that the atmospheric boundary layer wind tunnel testing is the most dependable approach for structural wind engineering. Such facilities have been widely utilized for the evaluation of wind loads on buildings and structures and the development of the current national wind codes and standards are mainly based on their outcomes. Recent interest in determining the wind loading for the design of solar panels has introduced pressure coefficient data mainly generated from wind tunnel studies. The literature data are subject to uncertainties owing to the experimental conditions and criteria followed in their experimental methodologies (Alrawashdeh and Stathopoulos, 2017).

Research to establish wind tunnel simulation criteria and approach for producing credible wind-induced pressures on solar panels is reported in this paper, which introduces the experimental procedure intended to investigate wind-induced pressure on solar arrays mounted on flat roofs of low-rise industrial buildings.

2. Overview and objectives

Wind effects on solar panels have been studied since the end of the seventies in the last century (Chevalien and Norton, 1979). Since

* Corresponding author.
E-mail address: h_alraw@encs.concordia.ca (H. Alrawashdeh)

https://doi.org/10.1016/j.jweia.2020.104339
Received 28 February 2020; Received in revised form 28 July 2020; Accepted 3 August 2020
Available online xxx
0167-6105/

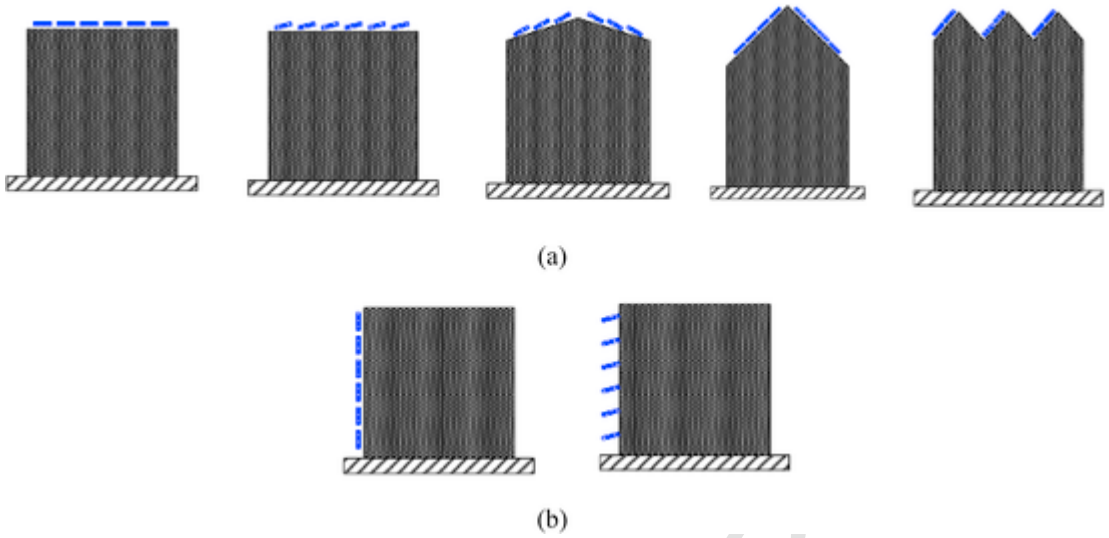

Fig. 1. Possible installations of solar panels into building's: (a) Roof, and (b) walls.

the turn of this century, there has been further growing interest in investigating wind-induced loads on solar panels, particularly utilizing atmospheric boundary layer wind tunnels for these studies. This has resulted in numerous parametric investigations, and a large quantity of data was incorporated into wind codes and standards to generate design provisions for roof-mounted solar panels.

Most of the studies available in the literature for solar panel systems were conducted for those mounted on flat-roofs (Wood et al., 2001; Ginger et al., 2011; Pratt and Kopp, 2012; Browne et al., 2013; Cao et al., 2013; Kopp, 2013; Stathopoulos et al., 2014; Naeiji et al., 2017; and Wang et al., 2018), while only a limited number of studies considered solar systems mounted on inclined roofs (Ginger et al., 2011; Naeiji et al., 2017; Aly and Bitsuamlak, 2014; Stenabaugh et al., 2015; and Leitch et al., 2016). Attention of the previous studies was particularly focused on solar panel systems mounted on industrial buildings with large plan dimensions (greater than 12.0 m) and height greater than 5.0 m.

Most of the previous studies were conducted in open-terrain exposure at geometric scales violating simulation requirements. Scales of 1:15 to 1:200 have been utilized for many reasons, such as to obtain larger geometries of solar panels that can be testable in the wind tunnel, to consider the flow between the solar panels and roofs under them, to increase the thickness of the panels for purpose of implanting pressure taps on both upper and lower surfaces and to have adequate space to fit the pressure tubes without disturbing the flow between the solar array and the roof. However, maintaining accurate model geometric scale is inherent to ensure the similarity of experimental conditions (e.g. turbulence integral scales, wind power spectra, Jensen numbers etc.) with those in the field.

Significant differences in values of the peak force coefficients have been found among the results of the previous studies. Also, analysis of the literature shows contradictory results reported on the influence of the major parameters on impacting wind-induced pressures on solar panel surfaces, such as: building size, array inclination and panel spacing. For example, it was found that wind loads on solar panels are strongly affected by building size (Stathopoulos et al., 2014; Banks, 2013; Kopp, 2013; and Pratt and Kopp, 2012). Banks (2013); Kopp (2013); and Pratt and Kopp (2012) have found that wind loads on solar panels increase with increasing the building size. However, Cao et al. (2013) have found that wind loads on solar panels are not affected by building size. Approach flow characteristics, building and solar panel configurations and dimensions as well as conditions of the experiments such as geometric test scaling and blockage ratio may be reasons for these discrepancies.

Literature studies carried out without any specific experimental criteria and requirements resulted in questionable results, and this was the impetus for the current study. Indeed, this study seeks to investigate the differences from comparisons of previous studies and, most importantly, to establish wind tunnel simulation criteria for producing credible wind-induced pressures on solar panels to be used for purposes of codification. A series of wind tunnel experiments have been devised to establish specific requirements for simulating roof-mounted solar panels in atmospheric boundary layer wind tunnels (ABLWTs), considering geometric test scaling as principal requirement to be examined. Models of three geometric test scales were designed and tested in an open country simulated atmospheric flow towards that end. The objective of the study was to quantify the differences found by enlarging the size of the model without changing the upstream simulation conditions which have been developed generally for a different geometric scale, i.e. a procedure that has applied routinely to several previous studies.

3. The wind tunnel experiments

All experiments for the present study have been carried out in the atmospheric boundary layer wind tunnel of Concordia University. The blow-down tunnel is of the open-circuit type with working section of 1.80 m in width, 12.2 m in length and has adjustable roof height in the range of 1.40–1.80 m. At the test section, the tunnel is equipped with a turntable of 1.60 m diameter through which the effect of different wind directions can be examined. Fig. 2 represents a photograph for the upstream view of the wind tunnel and the tested models.

A description of the design and performance of this experimental facility is sufficiently served by Stathopoulos (1984).

3.1. Wind tunnel modeling and flow simulation

A typical solar panel module used mainly for commercial installation (2 m by 1 m) has been considered for modeling. A system of roof solar array consists of 8 panels (rows), each 10 m long and 2 m wide, is designed for tilt angle of 15°. A 7.5 m high commercial building with plan dimensions of 14 m by 27 m is selected. The solar array is placed at setback distance of 2.0 m from the roof edges and a distance of 0.4 m above the roof – as illustrated in Fig. 3.

Three models are already set up at three geometric ratios (1:50, 1:100 and 1:200). All layout details shown in Fig. 3 are scaled down at the respective scale ratio, including the size of the gap underneath

Fig. 2. Upstream view of the wind tunnel with the tested models.

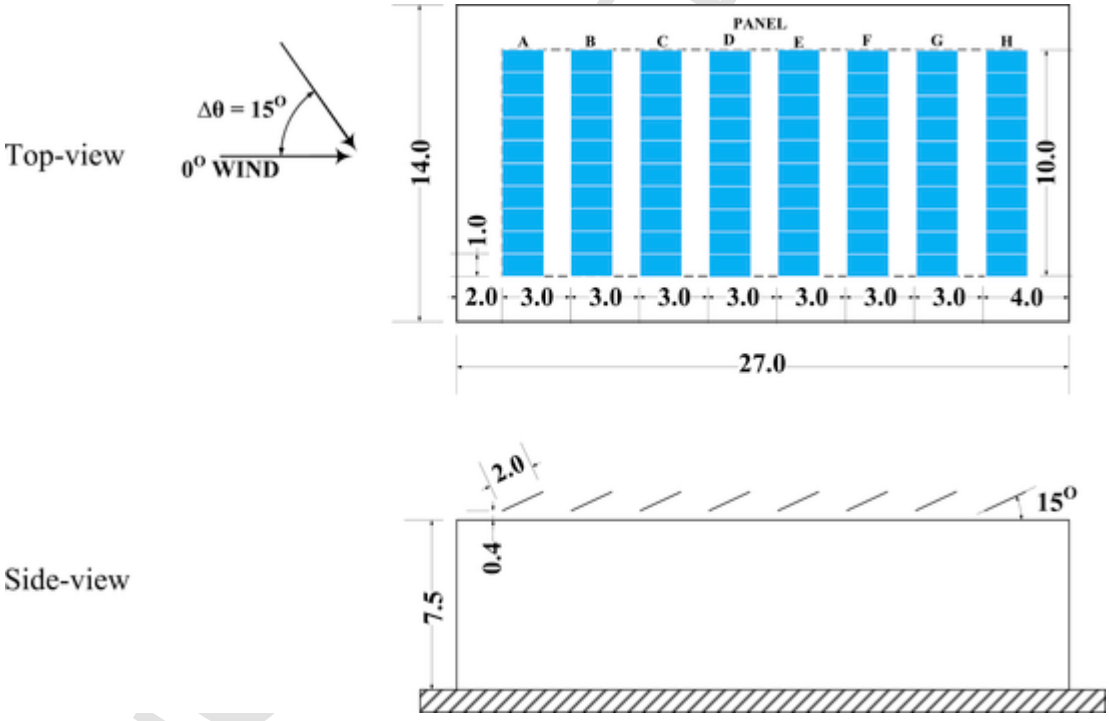

Fig. 3. Schematic illustration of the full-scale equivalent installation (dimensions in m).

the solar array, setback of the solar array and horizontal panel spacing. It should be noted that the model of 1:200 scale is the smallest testable model that could be manufactured so that the pressure taps can be inserted from both surfaces, while the model of 1:50 scale is the largest model that could be tested without distorting the wind tunnel blockage limit.

The three models of the considered arrays were made of thin "sandwiched metallic plates" of totally 2.3 mm thick – See Fig. 4 (a). Both surfaces (top and bottom) of each panel are equipped with pressure taps, identical in their distribution, to additionally determine the net wind pressures (force coefficients). The detailed distribution of the surface pressure taps for the models of the arrays at the considered geometric scales is illustrated in Fig. 4 (b). As shown, the solar panel models are equipped with a line of pressure taps at the middle with the exception of the largest model, which has been equipped with two additional lines close to the edges in order to investigate the effect of density of pressure taps per module. In the present study, the results will be confined only to pressure taps along the middle of the panels for comparison purposes.

(a)

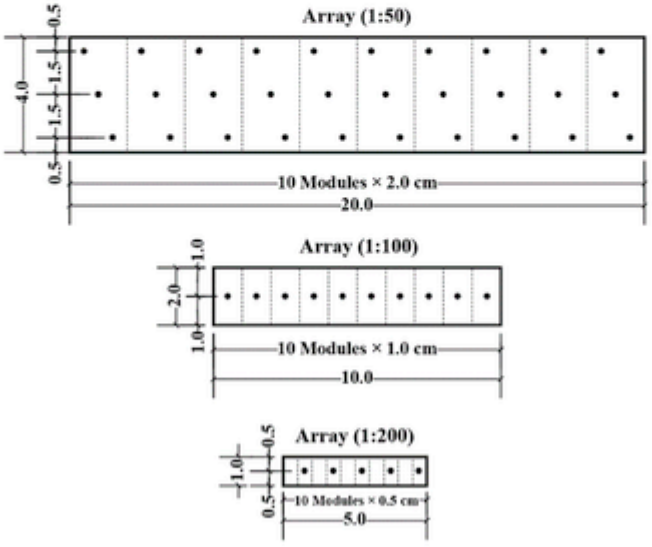

(b)

Fig. 4. (a) Close-up photographs for the solar panel of scale 1:50 and (b) Schematic illustration of solar panel models with pressure taps (dimensions in cm).

A traditional open-country exposure has been simulated at the test section of the wind tunnel. Fig. 5 (a) shows the approach flow profile of mean wind velocity and turbulence intensity at the test section measured using a 4-hole Cobra-probe (TFI). The mean wind speed variation at the test section is described by the log-law model and the measured velocity data best fit the velocity model with roughness length (z_o) of 0.01 cm in the wind tunnel. For the simulated wind profile, the scale is 1:500 considering a full-scale boundary layer thickness of 300 m.

3.2. Methodology

The modeling of wind effects on structures in wind tunnels requires, first and foremost, reproducing the characteristics of the natural wind and then correctly scaling down the structure to be tested. However, when it comes to test solar panels in simulated atmospheric boundary flow, selecting the geometric test scaling of the models to be tested is an experimental dilemma linked to the size of the solar panels prototype and some other layout features! Therefore, the designed models of different geometric scales (1:200, 1:100 and 1:50) were tested in the simulated atmospheric boundary layer flow to assess the impact of violating the test model size on wind-induced pressures of roof-mounted solar panels.

Landmark studies carried out on low-rise buildings by Lee (1975), Cook (1978), Holdø et al. (1982) and Stathopoulos and Surry (1983) have identified the longitudinal integral scale of turbulence ($L_{u,x}$) as an essential parameter for the simulated atmospheric boundary layer flow to reproduce realistic wind pressures. The scale of the turbulence itself should be considered in the selection of the geometric test scaling ensuring agreement of the turbulence of the approaching flow and the turbulence generated from the flow interaction with the bluff model. Particularly, the importance of accurately selecting the scale of the model (model size to prototype size) has been emphasized by Cook (1978), as follows:

> "*The linear scale of any building model should be matched to the longitudinal integral length scale, otherwise the scales of the simulated atmospheric turbulence and the building-generated turbulence will not match. In that event, the scaled dynamic response of the model in load or in deflection will not be correct.*"

This indicates that the integral length scale ($L_{u,x}$) of the turbulence to the building height (H) shall be the same in field (FS) and wind tunnel (WT), which can be expressed as follows:

$$\left(\frac{L_{u,x}}{H}\right)_{FS} = \left(\frac{L_{u,x}}{H}\right)_{WT} \quad (1)$$

in which,

$$L_{u,x} = 25\times(Z-d)^{0.35}\times z_o^{-0.063} \quad (2)$$

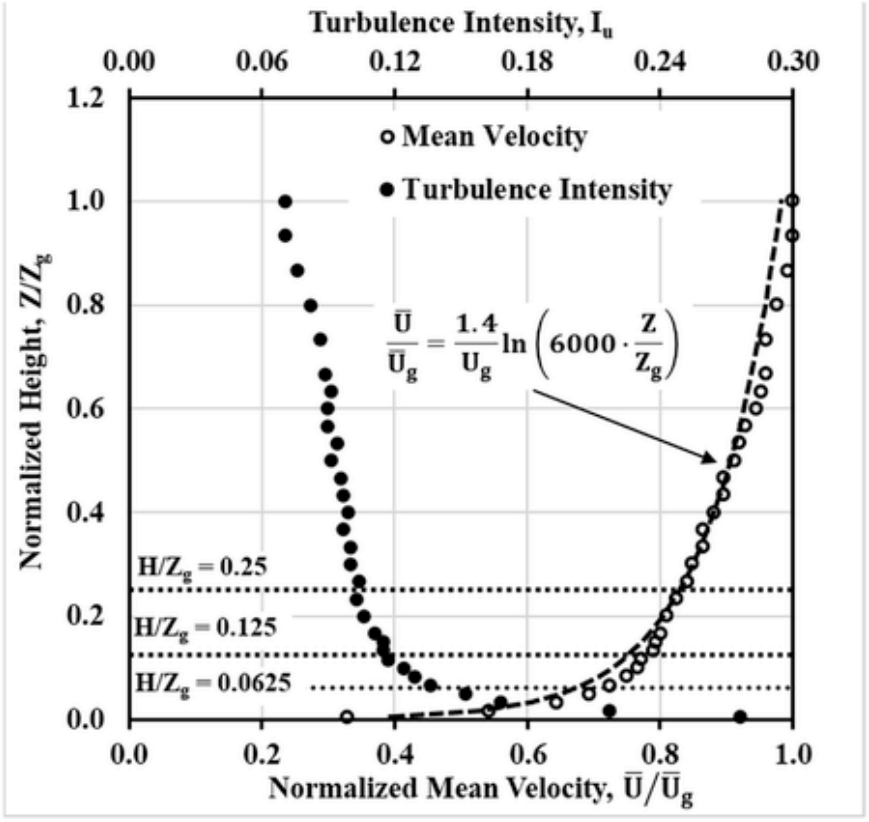

Fig. 5. (a) Vertical distribution of mean wind speed and longitudinal turbulence intensity and (b) Comparison of dimensionless spectrum measured at height $Z = Z_g/6$ with the counterpart models of von Kármán and Davenport.

z_o is the roughness length and d is the displacement height (Cook, 1978).

The longitudinal length scale of the simulated wind flow shown in Fig. 5 (a), based on the empirical model of the length scale of Cook (1978) provided in Eq. (2) for a geometric scale of 1:500, at the height $Z = Z_g/6$ cm (where Z_g is the gradient height, 60.0 cm) above the wind tunnel floor, is $L_{u,x} = 0.27$ m on the wind tunnel scale. As shown in Fig. 5 (b), the measured spectrum of the longitudinal wind tunnel flow (at $Z = Z_g/6$) shows favourable agreement with the corresponding empirical power spectrum model of Kármán (von Kármán, 1948) and the analytical model of Davenport (1961). It should be noted that von Kármán spectrum shown is generated for integral scale of $L_{u,x} = 135$ m in full-scale, which is 500 times larger than the corresponding value in the wind tunnel. Consequently, the simulated atmospheric boundary layer flow is appropriate for rightfully testing models at scales of 1:400 to 1:500, but adopting this scale is indeed out of the question as the solar panel model will be very small and untestable in the wind tunnel. The designed models of geometric scale 1:200, 1:100 and 1:50 are two and half-, five- and ten-fold the rightful size, respectively.

According to the similarity condition indicated by Eq. (1), testing the considered models in the simulated flow will respectively result in discrepancies of 2.5:1.0, 5.0:1.0 and 10.0:1.0 in the relevant turbulence scale ($L_{u,x}/H$) of the full-scale and the wind-tunnel – See Table 1.

Also, Table 1 shows that the wind tunnel models satisfy the experimental criteria recommended by the Wind Tunnel Testing for Buildings and Other Structures (ASCE/SEI 49, 2012). Thus, the maximum wind tunnel blockage ratio is lower than 5% and the minimum model Reynolds number is higher than 1.1×10^4. Blockage ratios are determined based on working section dimensions of the boundary layer wind tunnel of Concordia University (width = 180 cm and height = 160 cm).

3.3. Pressure measurements

The instantaneous wind pressures over the solar panel surfaces at the measurement pressure taps - see Fig. 4 (b) - are measured in the wind tunnel for all wind directions from 0° to 180° (as laid down in Fig. 3) in terms of time history wind load. The pressure measurements were carried out by connecting the pressure taps to a system of miniature pressure scanners made up of Scanivalve pneumatic modules (ZOC33/64Px), each capable of handling 64 pressure taps, and a digital service module (DSM 3400). The pressure scanners are calibrated to scan the pressure signals at frequency of 300 Hz for a total period of 27 s on wind-tunnel scale.

The surface pressure taps are connected to the channels of the Miniature Pressure Scanner using urethane tubing of 550 mm length. Traditional custom-made brass restrictors were placed within the tubes at 300 mm away from the pressure tap to add damping to minimize the Gain and Phase shifts of pressure signals – See Fig. 4 (a).

The measured pressures are normalized by the mean dynamic velocity pressure measured at reference height in order to place them in the form of non-dimensional pressure coefficients:

$$C_p(t) = \frac{P_{measured}(t)}{\bar{q}_H}, \quad \bar{q}_H = \frac{1}{2}\rho \bar{U}_H^2 \tag{3}$$

in which C_p is the instantaneous wind pressure coefficient of particular measurement tap either on top or bottom surface, $P_{measured}$ is the measured wind pressure at the tap, $\bar{q}_H$ is mean value of the dynamic velocity pressure at roof height (H), ρ is the density of the air and $\bar{U}_H$ is mean value of the wind velocity at roof height. The surface pressure coefficient is positive when the surface pressure acting as a pushing pressure; and negative, when acting as a suction.

The instantaneous force coefficient (local wind pressure across the solar module) is provided as the pressure difference between the top and bottom surfaces at a particular location,

$$C_F(t) = C_{P,Top}(t) - C_{P,Bottom}(t) \tag{4}$$

in which $C_{p,\,Top}(t)$ and $C_{p,Bottom}(t)$ are respectively the instantaneous wind pressure coefficients of the counterpart measurement taps on top and bottom surfaces of each module. It should be noted that the force coefficient is negative if the pressure tends to peel the solar panel away from the roof and positive when the pressure tends to push the array towards the roof.

Considering similarity requirements, geometric (H), time (T) and velocity (V) scales in the wind tunnel must be in parity with respective atmospheric conditions; therefore, the time scale of the pressure measurements are determined in combination with the geometric and velocity scales as follows:

$$\frac{T_W}{T_F} = \frac{V_F}{V_W} \times \frac{H_M}{H_F} \tag{5}$$

in which W, F and M refers to wind tunnel, full scale and model, respectively.

Accordingly, the time scale of the pressure measurement records of the tested geometric scales 1:50, 1:100 and 1:200, considering a velocity scale of approximately 1:3, are respectively 1:17, 1:34 and 1:68 so that the 27 s of pressure records are equivalent to 450, 900 and 1800 s in full-scale for the tested geometric scales. For "like-for-like" comparison, adjustments were applied to the pressure records associated with solar arrays of scales 1:50 and 1:100 to reference them to 1800-sec dynamic velocity pressure using well-known Durst curve (DURST, 1960).

Finally, repeatability tests were conducted with the three models to validate the integrity of the measured data.

Table 1
Experimental modeling parameters considered.

Model	Re × 10^4 Based on H	Max. Blockage Ratio (%)	$(H/z_o)_{WT}$	$\left(\frac{L_{u,x}}{H}\right)_{FS} : \left(\frac{L_{u,x}}{H}\right)_{WT}$
Large (1:50)	10.5	3.6	1500	10.0:1.0
Medium (1:100)	4.8	0.6	750	5.0:1.0
Small (1:200)	2.3	0.1	375	2.5:1.0

WT = Wind-tunnel and FS = Full-scale.

4. Experimental results and comparison

Experimental results reported in this section will be confined to the local mean and peak force coefficients along the middle of the panels of the considered arrays at inclination of 15°, which will be set against the geometric test scaling – recalling that the 1:200 array is the most rightful model, in that it is the most fulfilling for the requirement governing the model dimension and turbulence scale similarity. In this context, this would allow consideration of pressures deemed to be relevant in design provisions.

4.1. Mean and peak force coefficients

The impact of the geometric test scaling on the mean and peak force coefficients is examined. Fig. 6 shows the variation of the mean force coefficient (C_F) for modules positioned in the middle of the panels against the wind direction considering a pressure tap at the middle. Generally, the spatial distribution of the mean force coefficients at

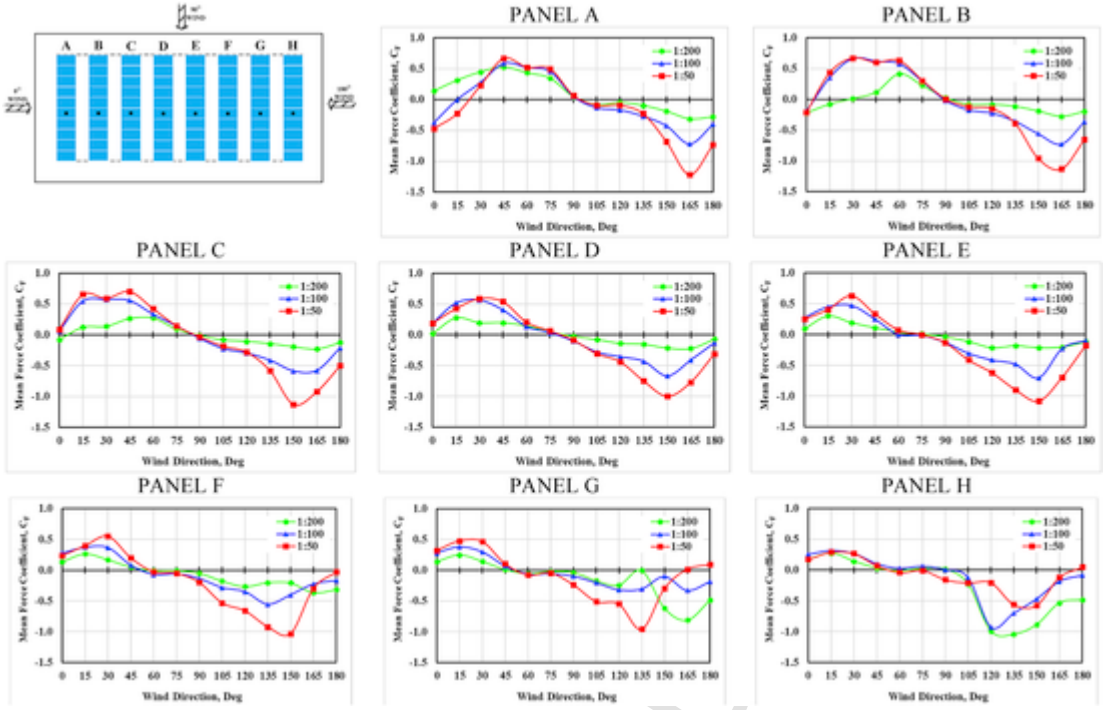

Fig. 6. Variation of mean force coefficient (C_F) at the middle of the panel (denoted by •) of 1:200, 1:100 and 1:50 array versus wind direction.

the considered geometric scales show volatile patterns among the wind direction.

Clearly, the modules of the front panel (A) of the smaller array experience a positive pressure for wind directions near perpendicular to the building edge (0°, 15° and 30°); whereas, the panel of the large models (1:100 and 1:50) experience negative wind pressure. For wind directions 30° and 45°, the entire array at the considered scales experiences positive pressure coefficients. With further changing the wind direction (i.e., 60°, 75° and 90° winds), the negative mean pressure coefficients appear on the modules of the downstream panels (E, F, G, H). For wind directions from 105° to 150°, the entire array at the considered scales is subjected to negative mean force coefficients. Similar observations were found for wind directions 165° and 180°, but the windward panels (G and H) of the 1:50 array experience positive mean pressure coefficients.

With emphasis on the mean force coefficient as it shows different patterns among the considered scales for wind blowing straight into the building edge (i.e., 0° and 180° winds), Fig. 7 presents the distribution of mean force coefficient (C_F) for 0° wind direction on the full-scale layout of the solar array. It is observed that the entire windward panel (A) of the 1:200 array experiences a positive pressure; whereas the corresponding larger panels of 1:100 and 1:50 arrays experience negative wind pressures. The leeward panels of the considered arrays experience positive mean pressure with higher values shown on the larger arrays (1:100 and 1:50). As a matter of fact, the negative mean force coefficients at scales 1:100 and 1:50 are declined rapidly on the windward panels (A and B) and the positive mean force coefficients appear on the downstream panels. On the other hand, the mean force coefficients of the 1:200 array show less spatial distribution disparity among the panels.

Indeed, the mean force coefficients show different patterns at the windward panel for flow straight into the building edge (A for 0° wind and H for 180° wind) – as illustrated in Fig. 6. However, for most panels and wind directions, the observed mean force coefficients increase with increasing the geometric test scaling. Generally, the mean force coefficients of the 1:50 array show little agreement with the 1:100 results, most likely found within a factor of 1.4. The results obtained on large arrays (1:100 and 1:50) approach poor level of concordance with the 1:200 array for the wind directions considered, in that the mean force coefficients are inflated by factors of 1.2–2.0 and 1.5–3.0, respectively.

Fig. 8 shows the variation of the negative and positive peak force coefficients of the panels' middle module with the wind direction. As shown, all panels of array scaled at 1:200 experience negative peak force coefficients for all wind directions. Nevertheless, some panels of larger arrays do not experience negative peak pressure coefficients, such as the leeward panels (E, F, G and H) for 0° and 15° winds; and some middle panels for 30° to 60° winds. Thus, there is inconsistency in the spatial distribution pattern of the negative peak force coefficients among the scales considered for array orientation between 0° and 75°. Therefore, the assessment of the negative peak pressure coefficients variability among the considered scales are restricted to those from wind direction ranging from 75° to 180°.

The negative peak force coefficients obtained on 1:100 and 1:50 arrays have generally approached slight levels of concordance (i.e., within a factor of 1.3) with the corresponding results obtained by 1:200 array for wind directions 75°, 90° and 105°. For winds from 120° to 180°, the results on the upstream panels (A, B, C, D and E) increase in magnitude with increasing the geometric test scaling but the exact opposite pattern is noted for the downstream panels (F, G and H). In general, the negative peak force coefficients obtained by 1:100 and 1:50 arrays are barely below the level of acceptable concordance with results of 1:200 array, showing an escalation factor ranging from 1.4 to 3.0 for the modules of the panels A to E and a reduction factor up to 3.0 on the modules of the panels F to H. On the other hand, the results of the 1:50 array for these wind directions attain a slight concordance with a factor of about 1.3 to the results of the 1:100 array.

With regard to the positive peak force coefficients, all panels of the array at the considered scales experience positive peak pressure for wind directions ranging from 0° to 105° – see Fig. 8. The positive peak force coefficients generally increase with increasing the geometric test scaling – except the modules of the front panel (A), where the posi-

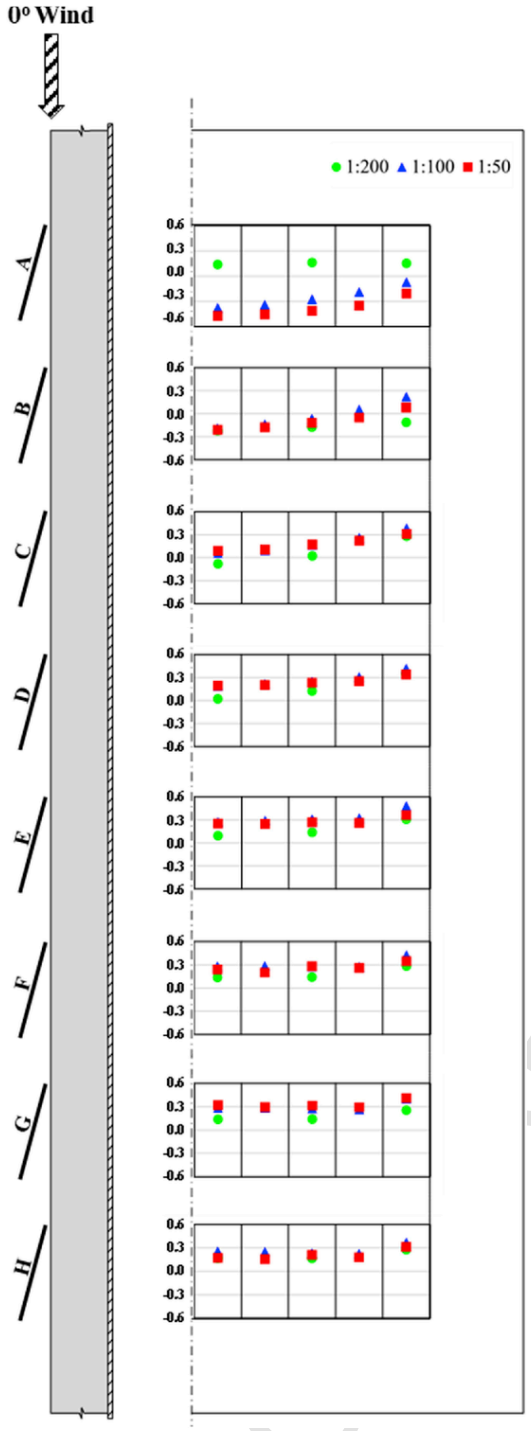

Fig. 7. Distribution of mean force coefficients (C_F) for 0° wind among the considered scales 1:200, 1:100 and 1:50 (array layout in full-scale).

tive peak force coefficients of 1:100 and 1:50 panels are lower than coefficients of the 1:200 panel. Generally, the peak force coefficients obtained on the 1:100 array approach a slight concordance with a 1.6 factor compared with the results of the 1:50 array. Also, the positive peak force coefficients of the 1:100 array show significant concordance (within a factor of 1.1) with the results obtained on the 1:200 array; on the other hand, the results of the larger array show less concordance with the results of 1:200 array - roughly greater by a factor ranging between 1.1 and 2.0.

4.2. Extreme force coefficients

The extreme results for the mean, positive peak and negative peak force coefficients, which represent the envelope values from the accounted wind directions, will be examined and compared in the light of relaxing the geometric test scaling. Indeed, the extreme results complied with this definition are the most substantial values of pressure coefficients as they are deemed to be design coefficients by some wind codes and standards (i.e., NBC, 2015; ASCE 7, 2016; and SEAOC, 2017). Therefore, it is important to follow up and assess the impact of the geometric test scaling on such values. Taking these measurements into consideration, it is also important to examine the most critical wind direction at which the extreme values were developed in order to capture all significant discussion points posed by the extreme force coefficients. In this respect, Figs. 9–12 show the values of extreme positive mean, negative mean, positive peak and negative peak force coefficients in conjunction with the corresponding most critical wind direction.

As illustrated in Fig. 9, the most critical wind direction for the extreme positive mean force coefficients show great similarity among the considered scales, where the extreme positive mean force coefficients often appear for wind directions ranging from 15° to 45°. The front-panel (A) mostly experiences extreme positive mean force coefficients for wind direction of 45°, subsequent panels (B and C) for 15°-45° winds, and downstream panels (D, E, F, G and H) for 15° wind.

On the other hand, the extreme positive mean force coefficients increase with further relaxing the geometric test scaling. As shown in Fig. 9, the extreme positive mean force coefficients obtained by the 1:200 array agree somewhat with the corresponding results obtained by the 1:100 and 1:50 arrays. Specifically, extreme mean force coefficients of the front- and back-panels of the 1:100 array are 1.2–1.5 times higher than the corresponding values of 1:200 results, while the results of the 1:50 array show higher factors (up to 2.0) compared with the results of the 1:200 array. Also, the results over the middle panels (B to G) of the 1:100 and 1:50 arrays were found to be about 1.5 and 2.0 times larger as compared with the results of the 1:200 array, respectively. Furthermore, the extreme positive mean force coefficients experienced by the 1:100 array were marginally greater than the results of the 1:50 array with a factor almost 1.1.

Fig. 10 presents the most critical wind directions for the negative mean force coefficients, which appear to be consistent for the three scales considered, all coming from wind directions ranging from 120° to 165°. The upstream panels (A, B and C) experience extreme negative mean force coefficients for winds 150° and 165°, middle panels (D, E, F and G) for 135°-165° and back-panel (H) for 120°-165° winds. The extreme negative mean force coefficients of the front panels (A to F) increase in magnitude with increasing the geometric test scaling, and vice versa for the extreme negative mean force coefficients of the back panels (G and H). The extreme negative mean force coefficients of the front-panels' modules of 1:100 array were significantly higher than the corresponding modules of 1:200 array; and certainly, the measurements of 1:50 array further worsened with the corresponding 1:200 array. On the other hand, extreme negative mean force coefficients of the back-panel modules (G and H) of 1:100 were respectively found to be in a factor of 0.4 and 0.8 compared with the results of the corresponding panels of the 1:200 array. Also, the results of the 1:50 array are found within factors of 1.3 and 0.4 with the corresponding extreme negative mean force coefficients of the panels G and H of 1:200 array, respectively. Finally, the extreme negative mean force coefficients of the 1:50 array are within a factor of 2.0–3.0 compared with the results of the corresponding modules of panels (A to G) of the 1:100 array; whereas, those of the back-panel of the 1:100 array are within a factor of 2.0 compared with the results of the panel (H) of the 1:50 array.

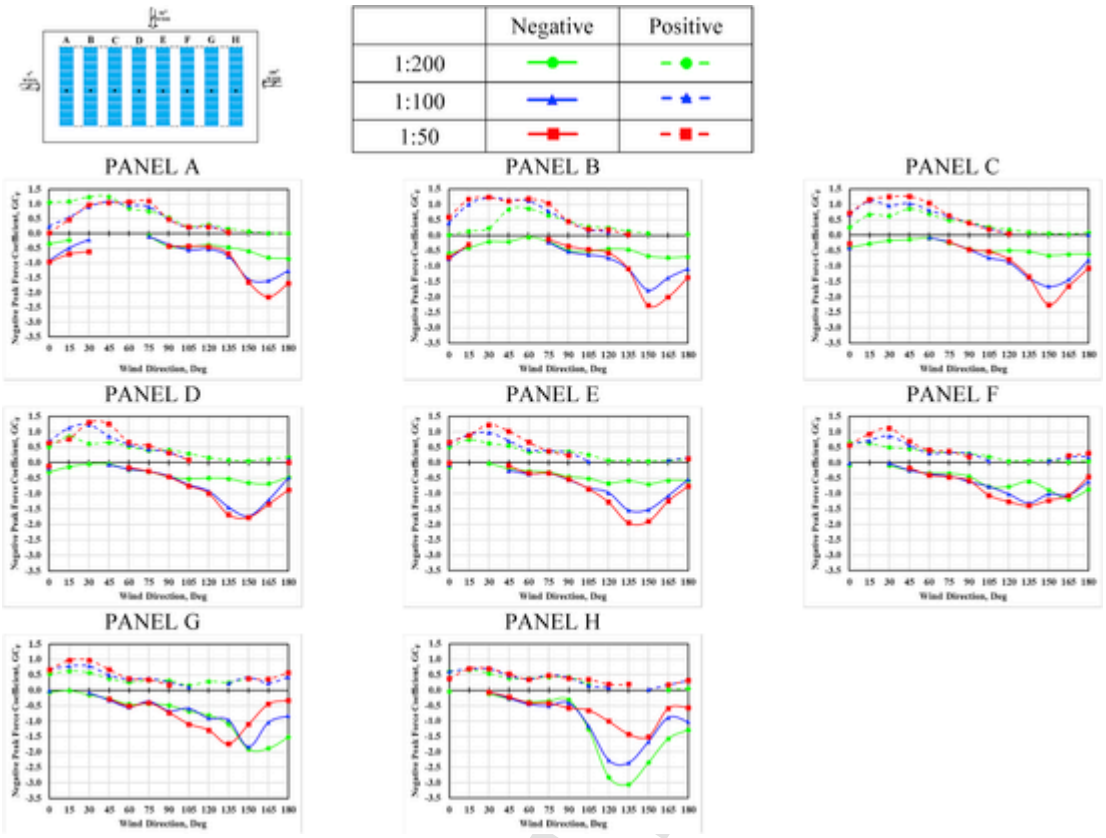

Fig. 8. Variation of negative and positive peak force coefficient (GC_F) at the middle of the panel (denoted by ▪) of 1:200, 1:100 and 1:50 array versus wind direction.

As presented in Figs. 11 and 12, the most critical wind directions for the extreme positive and negative peak force coefficients show significant agreement for the geometric test scales considered. The front-panel of the considered arrays experience extreme negative peak force coefficients for wind directions ranging from 30° to 60°, the upstream middle-panels (B and C) for 15° to 45° and the downstream panels (D, E, F, G and H) for 15° and 30°. As also illustrated in Fig. 12, the most critical wind direction for extreme negative peak force coefficients are evidently generated for wind directions ranging from 120° to 165°.

On the other hand, the extreme positive and negative peak force coefficients demonstrated pattern almost similar to the extreme mean force coefficients; thus, they are visibly different among the considered scales at varying degrees in accordance with the module location – qualitatively summarized with enlarging the size of the model as follows: Under-designed front and back edge modules and overdesigned interior modules against the positive loadings; Under-designed back modules and overdesigned front and interior modules against the negative loadings. For positive and negative loadings, the edge modules have remained consistent among the geometric test scales. Certainly, the data provided in Figs. 11 and 12 are useful to the designers to estimate the possible discrepancies involved when using data originating from studies distorting scaling requirements for wind tunnel testing.

5. Conclusions

This paper concisely discusses the knowledge available on wind loads on solar panels mounted on flat roofs and points out the disagreement over the results of past studies in this area. In this regard, the paper has introduced the experimental procedure implemented to examine the impact of relaxing the geometric test scaling on wind loads on roof-mounted solar panels tested in atmospheric boundary layer wind tunnel. Several tests were carried out on models at geometric test scaling of 1:200, 1:100 and 1:50 in a fully developed atmospheric flow, thereby providing two and half-, five- and ten-fold the rightful model size.

Comparisons made to examine to what extent such experimental acts affect the force coefficients confirmed that relaxing the geometric test scaling results in:

- Inflating the mean force coefficients, the front panels' negative peak force coefficients and the positive peak force coefficients – results may be conservative.
- Lowering the negative peak force coefficients of the back panels – results may be unconservative.
- Minimal influence on the most critical wind direction.
- Overvaluing and undervaluing tendencies, depending on panel location, of the design force coefficients, including extreme negative and positive values with variations by a factor up to 3.5.

The present study recommends that caution needs to be exercised when testing solar panels in ABLWTs, that is ensuring the ratio of the model height to the turbulence scale size shall be preserved constant with natural wind. Beside setting that as a challenge, research to develop a possible correction methodology would be of great interest.

Uncited reference

Karman, 1948

Declaration of competing interest

The authors declare that they have no known competing financial interests or personal relationships that could have appeared to influence the work reported in this paper.

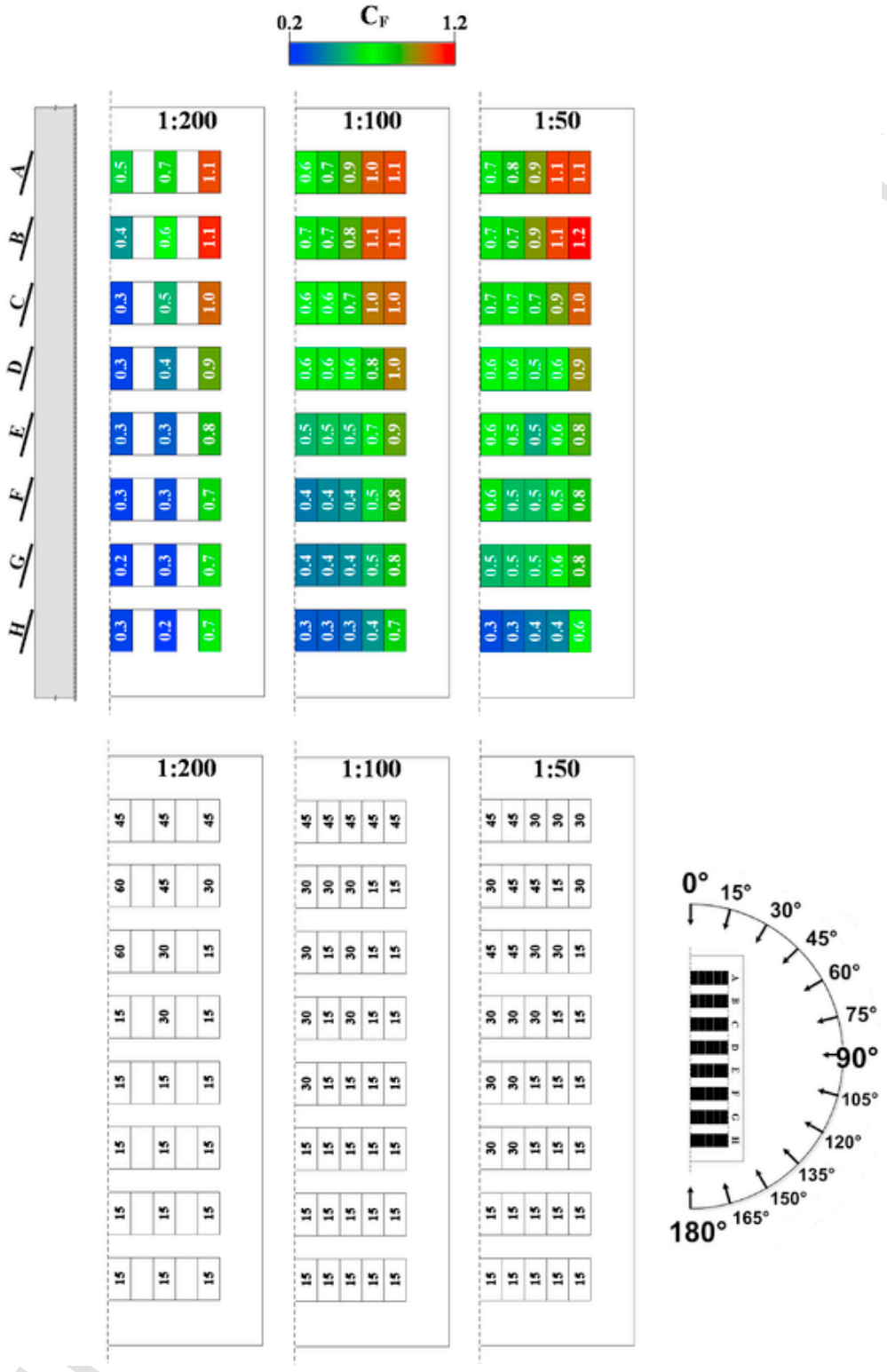

Fig. 9. Extreme positive mean force coefficient and the corresponding most critical wind direction for the tested models 1:200, 1:100 and 1:50 (array layout in full-scale).

Acknowledgment

The authors gratefully express their appreciation for the financial support from the Natural Sciences and Engineering Research Council of Canada (NSERC) for the present research.

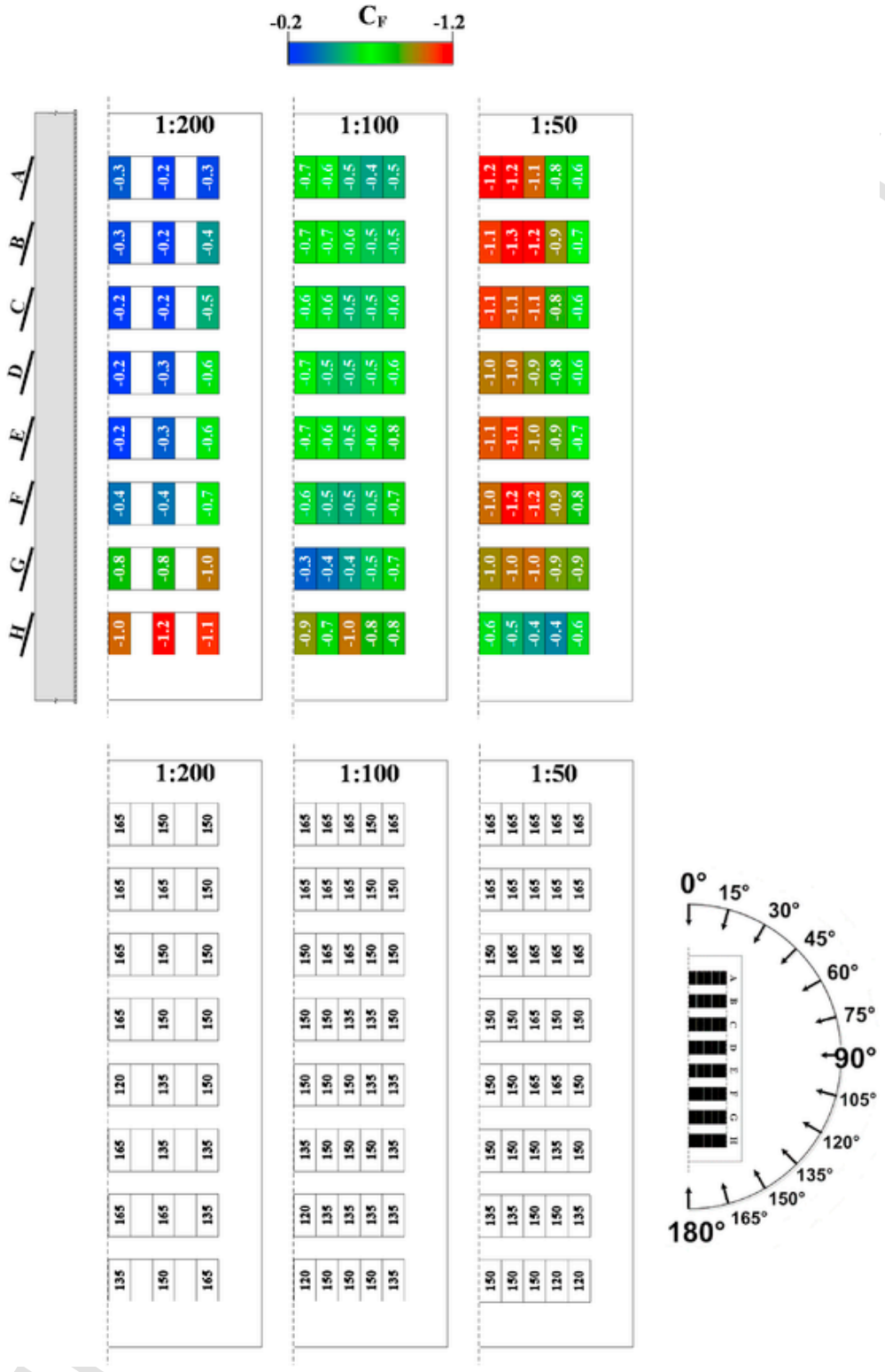

Fig. 10. Extreme negative mean force coefficient and the corresponding most critical wind direction for the tested models 1:200, 1:100 and 1:50 (array layout in full-scale).

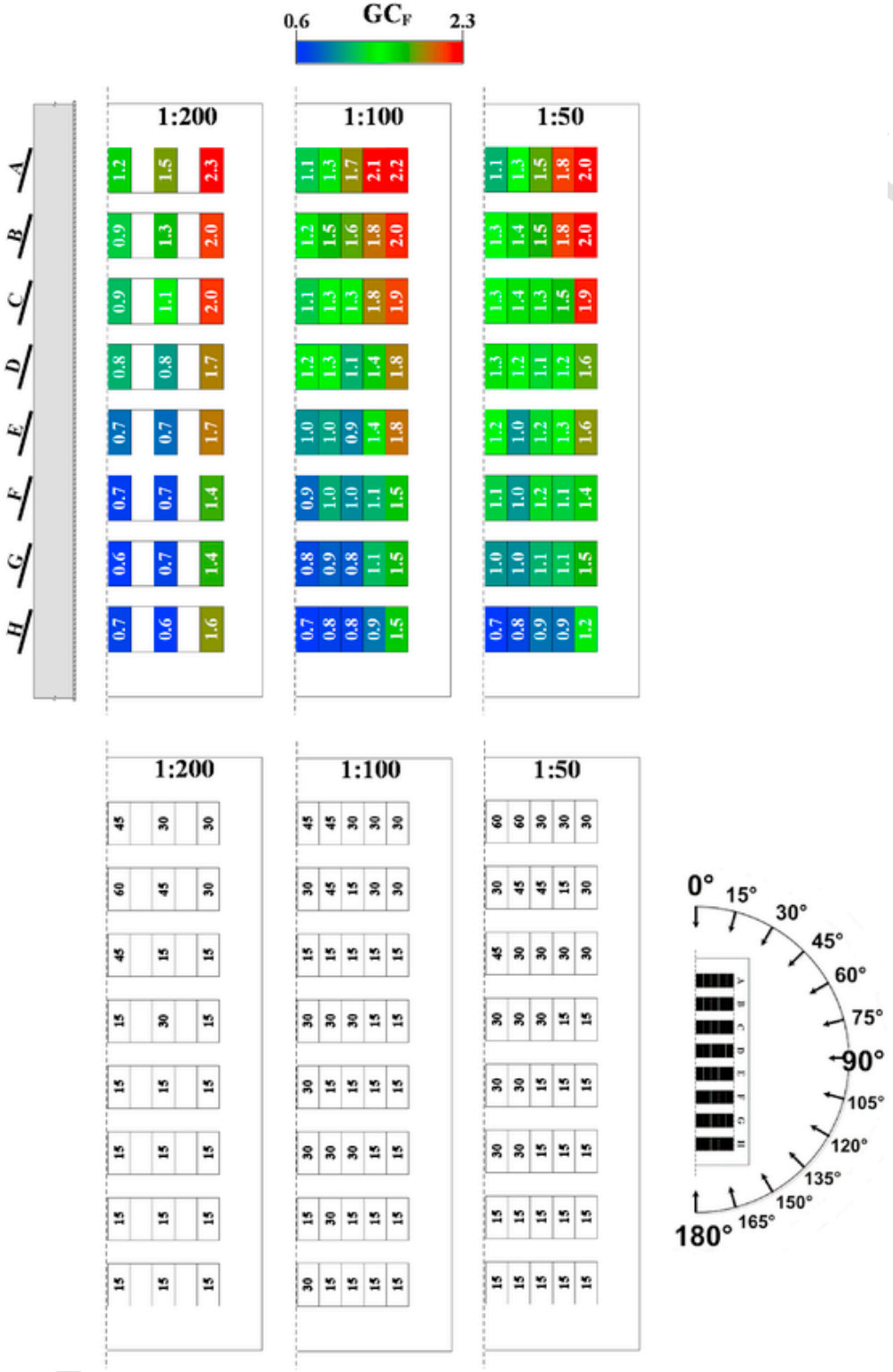

Fig. 11. Extreme positive peak force coefficient and the corresponding most critical wind direction for the tested models 1:200, 1:100 and 1:50 (array layout in full-scale).

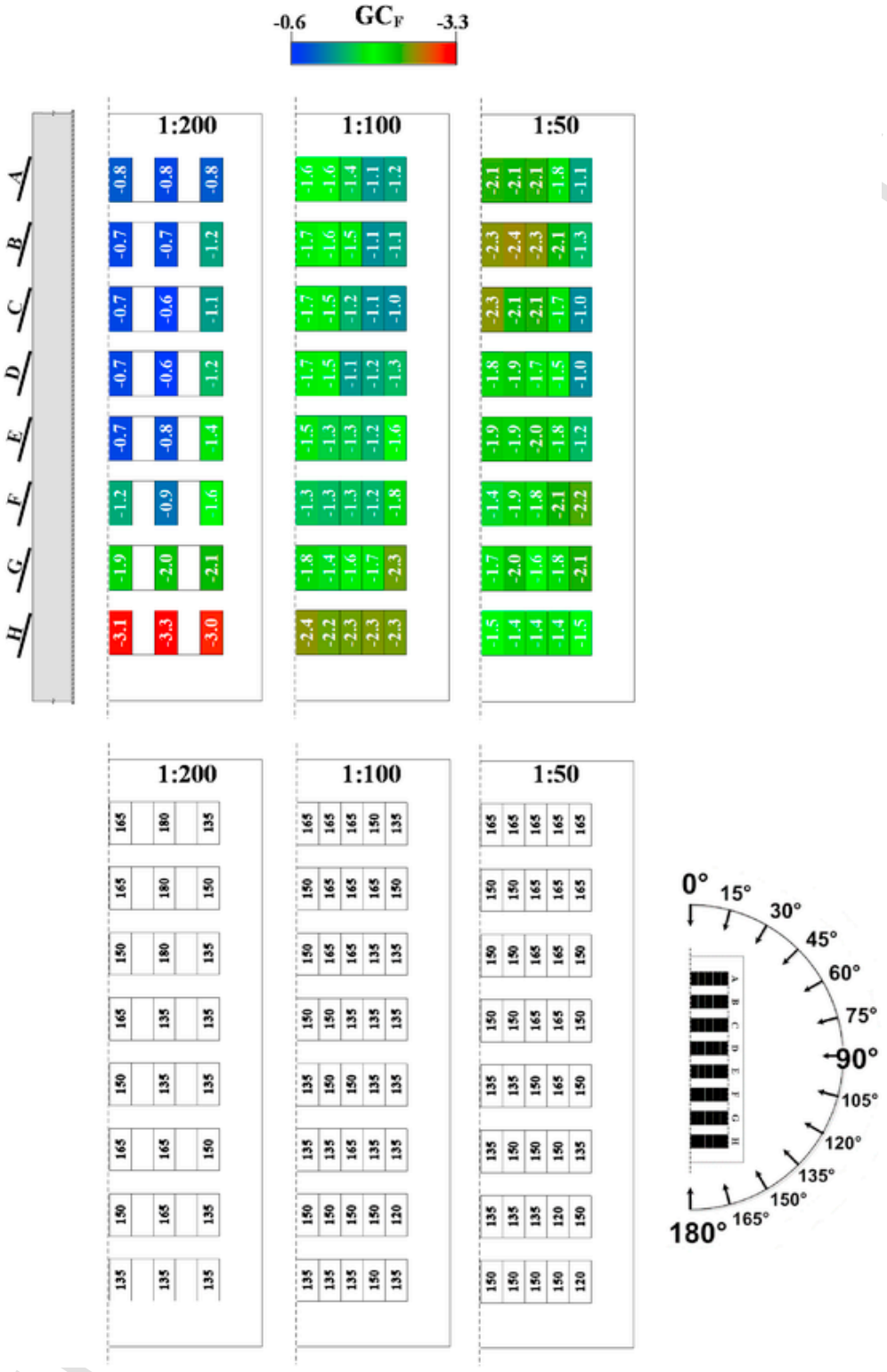

Fig. 12. Extreme negative peak force coefficient and the corresponding most critical wind direction for the tested models 1:200, 1:100 and 1:50 (array layout in full-scale).

References

Alrawashdeh, H, Stathopoulos, T, 2017. Wind effects on roof-mounted solar panels. In: Proceedings of the 2nd Coordinating Engineering for Sustainability and Resilience (CESARE'17), Amman, Jordan, May 3-8, 2017.

Aly, A M, Bitsuamlak, G, 2014. Wind-induced pressures on solar panels mounted on residential homes. J. of Archit Eng. 20.

ASCE/SEI 49, 2012. Wind Tunnel Testing for Buildings and Other Structures. American Society of Civil Engineers (ASCE 49–12). Reston, VA.

ASCE/SEI 7-16, 2016. Minimum Design Loads for Buildings and Other Structures. Structural Engineering Institute of ASCE. Reston, VA.

Banks, D, 2013. The role of corner vortices in dictating peak wind loads on tilted flat solar panels mounted on large, flat roofs. J. Wind Eng. Ind. Aerod. 123, 192–201.

Browne, M T L, Gibbons, M P M, Gamble, S, Galsworthy, J, 2013. Wind loading on tilted roof-top solar arrays: the parapet effect. J. Wind Eng. Ind. Aerod. 123, 202–213.

Cao, J, Yoshida, A, Saha, P K, Tamura, Y, 2013. Wind loading characteristics of solar arrays mounted on flat roofs. J. Wind Eng. Ind. Aerod. 123, 214–225.

Chevalien, L, Norton, J, 1979. Wind Loads on Solar Collector Panels and Support Structure, Aerospace Engineering Department. Texas A&M University.
Cook, N J, 1978. Determination of the model scale factor in wind-tunnel simulations of the adiabatic atmospheric boundary layer. J. Wind Eng. Ind. Aerod. 2, 311–321.
Davenport, A G, 1961. The spectrum of horizontal gustiness near the ground in high winds. Q.J.R. Meteorol. Soc. 87, 194–211.
Durst, C S, 1960. Wind speeds over short periods of time. Meteorol. Mag. 89, 181–187.
Ginger, J, Payne, M, Stark, G, Sumant, B, Leitch, C, 2011. Investigation on Wind Loads Applied to Solar Panels Mounted on Roofs. Cyclone Testing Station. School of Engineering & Physical Sciences, James Cook University, Townsville.
Holdø, A E, Houghton, E L, Bhinder, F S, 1982. Some effects due to variations in turbulence integral length scales on the pressure distribution on wind-tunnel models of low-rise buildings. J. Wind Eng. Ind. Aerod. 10, 103–115.
Karman, T Von, 1948. Progress in the statistical theory of turbulence. Proc. Natl. Acad. Sci. U.S.A. 34 (11), 530–539.
Kopp, G A, 2013. Wind loads on low-profile, tilted, solar arrays placed on large, flat, low-rise building roofs. J. Struct. Eng.-ASCE 140.
Lee, B E, 1975. Some effects of turbulence scale on the mean forces on a bluff body. J. Wind Eng. Ind. Aerod. 1, 361–370.
Leitch, C J, Ginger, J D, Holmes, J D, 2016. Wind loads on solar panels mounted parallel to pitched roofs, and acting on the underlying roof. Wind Struct. 22, 307–328.
Naeiji, A, Raji, F, Zisis, I, 2017. Wind loads on residential scale rooftop photovoltaic panels. J. Wind Eng. Ind. Aerod. 168, 228–246.
NBC, 2015. User's Guide-NBC 2015, Structural Commentaries (Part 4). Issued by the Canadian Commission on Buildings and Fire Codes. National Research Council of Canada.
Pratt, R N, Kopp, G A, 2012. An initial study of the aerodynamics of photovoltaic panel arrays mounted on large flat roofs. In: The Seventh International Colloquium on Bluff Body Aerodynamics and Applications (BBAA7) Shanghai, China. pp. 2–6.
SEAOC, 2017. Wind Design for Solar Arrays. SEAOC Report PV2–2017. Structural Engineers Association of California. Sacramento, California.
Stathopoulos, T, 1984. Design and fabrication of a wind tunnel for building aerodynamics. J. Wind Eng. Ind Aerod. 16, 361–376.
Stathopoulos, T, Surry, D, 1983. Scale effects in wind tunnel testing of low buildings. J. Wind Eng. Ind. Aerod. 13, 313–326.
Stathopoulos, T, Zisis, I, Xypnitou, E, 2014. Local and overall wind pressure and force coefficients for solar panels. J. Wind Eng. Ind. Aerod. 125, 195–206.
Stenabaugh, S E, Iida, Y, Kopp, G A, Karava, P, 2015. Wind loads on photovoltaic arrays mounted parallel to sloped roofs on low-rise buildings. J. Wind Eng. Ind. Aerod. 139, 16–26.
Wang, J, Yang, Q, Tamura, Y, 2018. Effects of building parameters on wind loads on flat-roof-mounted solar arrays. J. Wind Eng. Ind. Aerod. 174, 210–224.
Wood, G S, Denoon, R O, Kwok, K C S, 2001. Wind loads on industrial solar panel arrays and supporting roof structure. Wind Struct. 4, 481–494.